NeuroImage 188 (2019) 161–170

Contents lists available at ScienceDirect

NeuroImage

journal homepage: www.elsevier.com/locate/neuroimage

Evaluation of a dual signal subspace projection algorithm in magnetoencephalographic recordings from patients with intractable epilepsy and vagus nerve stimulators

Chang Cai [a], Jiajing Xu [a], Jayabal Velmurugan [a,b,c,d], Robert Knowlton [g], Kensuke Sekihara [e,f], Srikantan S. Nagarajan [a,*], Heidi Kirsch [a,g]

[a] Department of Radiology and Biomedical Imaging, University of California, San Francisco, CA, 94143-0628, USA
[b] Department of Clinical Neurosciences, National Institute of Mental Health and Neurosciences, Bangalore, India
[c] MEG Research Center, National Institute of Mental Health and Neurosciences, Bangalore, India
[d] Department of Neurology, National Institute of Mental Health and Neurosciences, Bangalore, India
[e] Department of Advanced Technology in Medicine, Tokyo Medical and Dental University, 1-5-45 Yushima, Bunkyo-ku, Tokyo 113-8519, Japan
[f] Signal Analysis Inc., Hachioji, Tokyo, Japan
[g] Department of Neurology, University of California, San Francisco, CA 94143-0628, USA

ARTICLE INFO

Keywords:
Brain mapping
Magnetoencephalography
DSSP
Intractable epilepsy
Vagus nerve stimulators

ABSTRACT

Magnetoencephalography (MEG) data is subject to many sources of environmental noise, and interference rejection is a necessary step in the processing of MEG data. Large amplitude interference caused by sources near the brain have been common in clinical settings and are difficult to reject. Artifact from vagal nerve stimulators (VNS) is a prototypical example. In this study, we describe a novel MEG interference rejection algorithm called dual signal subspace projection (DSSP), and evaluate its performance in clinical MEG data from people with epilepsy and implanted VNS. The performance of DSSP was evaluated in a retrospective cohort study of patients with epilepsy and VNS who had MEG scans for source localization of interictal epileptiform discharges. DSSP was applied to the MEG data and compared with benchmark for performance. We evaluated the clinical impact of interference rejection based on human expert detection and estimation of the location and time-course of interictal spikes, using an empirical Bayesian source reconstruction algorithm (Champagne). Clinical recordings, after DSSP processing, became more readable and a greater number of interictal epileptic spikes could be clearly identified. Source localization results of interictal spikes also significantly improved from those achieved before DSSP processing, including meaningful estimates of activity time courses. Therefore, DSSP is a valuable novel interference rejection algorithm that can be successfully deployed for the removal of strong artifacts and interferences in MEG.

1. Introduction

From the time of its first introduction, magnetoencephalography (MEG) has been used to map functional brain activity noninvasively with good spatial and excellent temporal resolution, and thus to offer valuable information for use in clinical neurology and basic neuroscience. However, MEG has suffered from an important shortcoming: it is prone to contamination from signals other than the signals of interest - including inevitable non-biological sources like power lines and trains, and biological sources outside of the brain like the heart. Though most of this interference is of similar magnitude to brain activity, some of it is high amplitude and needs special attention - including artifact from dental work, and especially interference from vagal nerve stimulators (VNS), relatively common in people with intractable epilepsy, that makes it very difficult for us to see and then to model activity of interest (Nagarajan et al., 2006a; Taulu and Simola, 2006; Sekihara et al., 2016).

A variety of methods have been used to minimize artifact in magnetoencephalographic recordings with varying degrees of success. Averaging responses over trials is one method commonly used; this takes advantage of the idea that interference in different trials is statistically independent, whereas evoked signals are not. However, this method requires a large number of trials, and evoked signals must be relatively

* Corresponding author.
E-mail addresses: sri@ucsf.edu (S.S. Nagarajan), Heidi.Kirsch@ucsf.edu (H. Kirsch).

https://doi.org/10.1016/j.neuroimage.2018.11.025
Received 30 July 2018; Received in revised form 22 October 2018; Accepted 16 November 2018
Available online 29 November 2018
1053-8119/

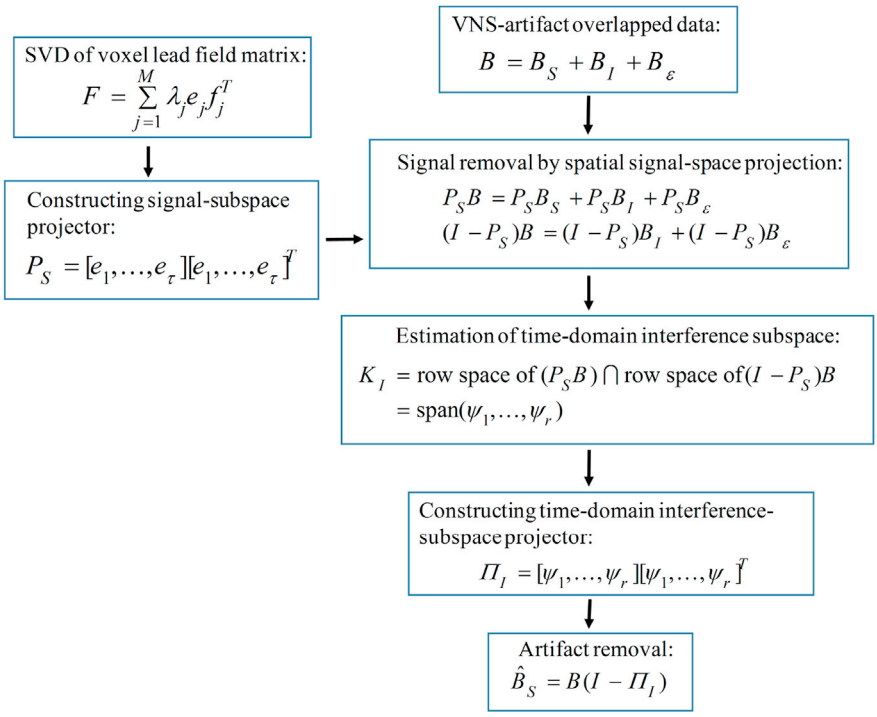

Fig. 1. Schematic showing the processing steps of DSSP.

similar and robust (Nagarajan et al., 2007a). Filtering is another widely applied method, but requires prior knowledge about the interference. Recently, data-driven approaches such as principal component analysis (PCA), independent component analysis (ICA) have been popular. However, these methods ask users to make subjective choices during application (e.g. choice of threshold in PCA and of interference component in ICA), and the methods cannot exploit pre-/poststimulus partitioning of the data (Ossadtchi et al., 2004; Nagarajan et al., 2006b). Joint decorrelation is another method commonly supposed to be robust to many types of interference problems, but its use requires the design of different bias filters for different interference types, and thus to some extent requires prior knowledge of the interference (de Cheveigné and Parra, 2014). Algorithms based on statistical properties of the interference are a class of automated interference algorithm method hailed as both reliable and robust. The partitioned factor analysis (PFA) algorithm (Nagarajan et al., 2006a, 2007b; Zumer et al., 2008) is implemented by obtaining a probabilistic model from the data distributions in the pre-stimulus period (when the interference exists) and the post-stimulus period (when both interference and true signal exist), and then inferring model parameters from these distributions. This method handles most types of interference well, but since it relies on the availability of separate measurements that capture the statistical properties of the interference, its use is limited to situations where such separate measurements are appropriate, and it is not effective for removing overlapped interference (Nagarajan et al., 2007a). Also, these algorithms may not be effective for interference of extremely large magnitude relative to the signals being estimated, which is often seen in MEG data in patients with VNS implants.

Artifacts of significant magnitude are not rare in MEG recordings, and resolving MEG data from distorted recordings is often of great clinical significance. Particularly in the case of people with intractable epilepsy who have received VNS implants and have continued refractory focal onset seizures, MEG studies are an important part of the evaluation for and the planning of resective surgery. Without interference rejection, MEG data in many people with VNS implants will be completely distorted by significant artifact from the stimulator and the lead-wires, making it extremely difficult to see interictal epileptiform activity or stimulus evoked responses from primary sensory cortices, thus diminishing the usefulness of MEG for these patients and, thereby, their hope for recovery (Sekihara et al., 2016). Therefore, developing and testing algorithms for interference rejection in MEG data is important, especially new algorithms that specifically address the kind of interference that is not well handled by currently available options but that is clinically important (e.g. VNS implant interference). Ideally such an algorithm would be robust and broadly capable of rejection of as many types of interference as possible. Given that many source localization platforms include lead fields, it would be ideal to offer a tool that is also based on lead fields. Right now options are restricted to specific hardware platforms. For example, the temporally extended signal space separation method (tSSS) developed by one MEG manufacturer offers a potential solution (Taulu and Hari, 2009) but this tool has only been demonstrated for the Elekta platform and has not been shown for other platforms. In contrast, here we show a MEG hardware platform independent algorithm for large interference rejection.

Dual signal subspace projection (DSSP) is a newly proposed algorithm for removal of large interference in biomagnetic measurements, and has the potential to handle many different kinds of interference (Sekihara et al., 2016). DSSP is based on the fact that MEG signal has both spatial and temporal properties. This allows us to define a signal subspace in the space domain, and another signal subspace in the time domain. We assume that the interference signal is present all the time across the whole signal subspace, either inside or outside the spatial-domain signal subspace, or both. In contrast, activity from the brain is presumed to exist only inside the spatial domain signal subspace. The DSSP algorithm first projects the columns of the measured data matrix onto the inside and outside of the spatial-domain signal subspace, creating two 'projected' data matrices. The intersection of the row spans of these two 'projected' matrices is then taken to be an estimate of the time-domain interference subspace, and artifact removal is carried out on the basis of this estimated interference subspace. Details of the DSSP algorithm have been published recently, but the performance of DSSP in assisting the identification and localization of epileptiform discharges has not been determined. In this paper we evaluate its ability in these arenas, using subject specific lead fields and selecting parameters, exploring its capability to handle various

Table 1
Clinical characteristics of ten subjects. Note that some patients were referred from outside institutions and thus their information was limited to that available at the time of the MEG scan.

ID	Age	Duration of Epilepsy	MR abnormality	Ictal EEG	Interictal EEG	PET CT	Presumed EZ	Interictal MEG spikes	Num of spikes before DSSP	Num of spikes after DSSP	Max field strength Before DSSP (pT)	Max field strength after DSSP (pT)	Notes
1	22	18	Left lateral frontal lobe cortical dysplasia	Poorly localized; left frontocentral region	Left frontocentral spikes or polyspikes	Normal but PET fusion with MRI corresponding hypometabolism	Left frontal onset	Left frontotemporal	0	39	70.2	2.3	
2	25	20	Primary read as normal, secondary read as bilateral posterior pachygyria	Seizures arising independently from each hemisphere; poorly localized	Independent bitemporal spikes; generalized paroxysmal fast actvity	Negative	Unknown to date	Bilateral slow waves model bilaterally in the suprasylvian frontal and infra-sylvian temporal lobes	44	33	5.3	2.8	
3	44	32	Unremarkable	Not available	Right temporal sharp waves, generalized spike and polyspike discharges	N/A	Unknown to date	Right temporal, right frontal	107	168	148.3	4.8	
4	22	20	Encephalomalacia of the left temporal lobe, volume loss of left hippocampus	Left parietal region	Left TIRDA, frequent broad spikes over left temporo-parietal region, occasional left anterior temporal predominance	N/A	Left temporo-parietal-occipital	Posterior medial left temporal lobe	3	100	48.3	2.5	Prior posterior temporal resection
5	17	Not available	Left hipopcampal atrophy, left hemispheric cortical dysplasia	Left hemisphere onset	Intermittent left frontotemporal discharges	Hypometabolism of left temporal lobe, left parietal lobe, left posterior occiptal lobe	Left hemisphere, probable left temporal lobe	Left temporal region	47	143	60.5	2.1	
6	38	17	Left parietal, left temporal	Independent bilateral frontotemporal	Independent right and left temporal discharges	Bilateral temporal hypometabolism	Frontal or temporal; laterality unknown	None	5	14	21.1	2.0	
7	31	25	Unremarkable	Vertex spike followed by diffuse fast activity	Bilateral central/ paracentral regions	N/A	Unknown to date	Right cingulate gyrus; L > R perirolandic regions	35	54	61.9	1.6	
8	37	19	T2/FLAIR hyperintensity and atrophy of bilateral temporal lobes, $L > R$	Left frontotemporal	Left anterior temporal; also rare right temporal spikes	Bilateral temporal hypometabolism	Left mesial temporal	Right temporal spikes, rare left temporal spikes	24	32	32.0	1.8	
9	26	Since young	Expected changes from medial left frontal lobe corticectomy; otherwise unremarkable	Poorly localized and lateralized; some with preceding left parasagittal sharp waves	No interictal	N/A	Frontal; lateralization unclear but more likely left	None	43	72	56.6	1.1	
10	28	27	Left parietal cavernous malformation	Suggestive of frontal onset but poorly lateralized	Bifrontal sharp waves, left frontal spikes	Increased metabolic activity in high left posterior pariental sulcus	Unknown to date	Right suprasylvian frontal lobe	3	53	116.7	2.6	

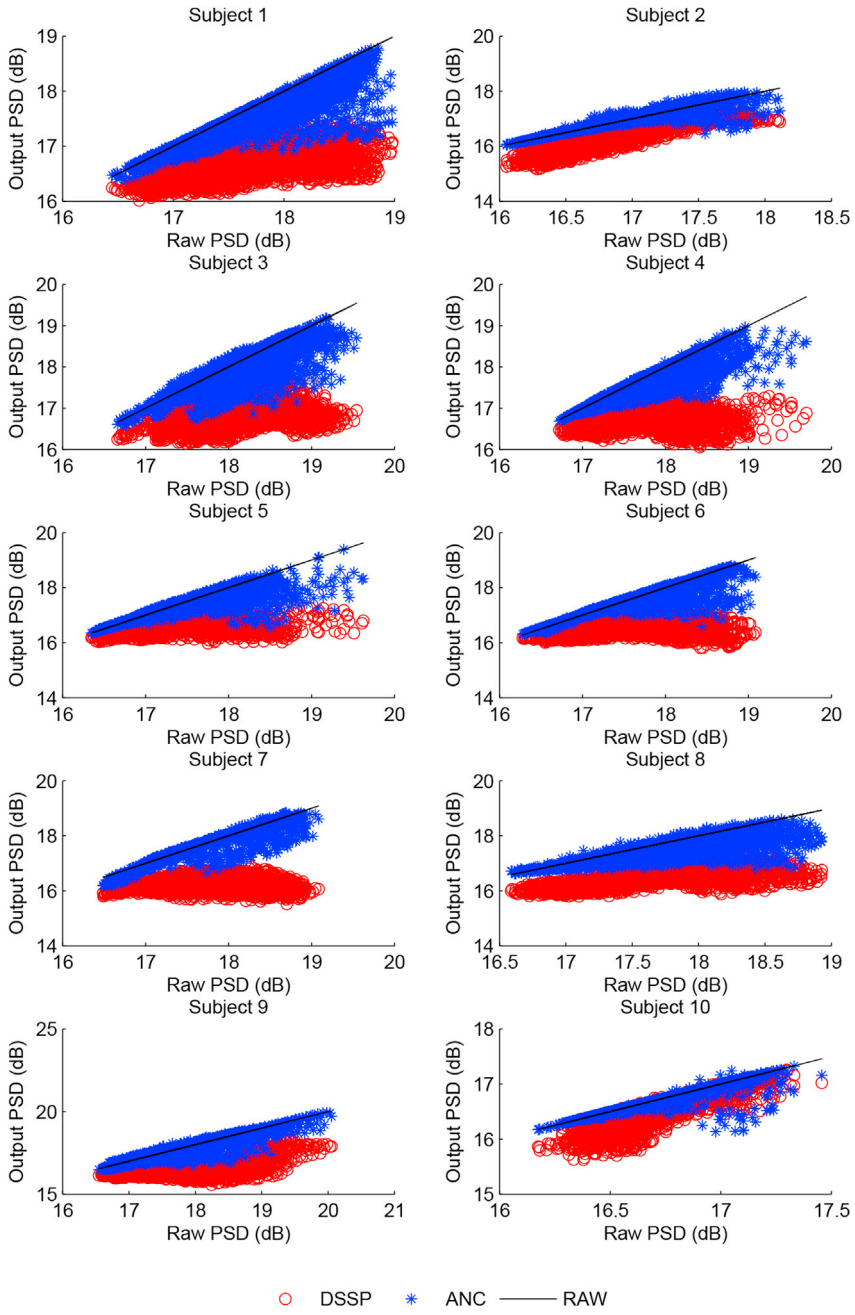

Fig. 2. Each panel shows the power spectral density (PSD) for each channel before and after either DSSP (red dots) or ANC (blue dots), for each of the ten subjects in this study. Points along the diagonal line in each panel indicates lack of interference rejection.

artifacts as part of processing of clinical datasets. In particular, we will evaluate whether it will be helpful to solve the problem of spike detection in patients with VNS implants. We will also test its ability to improve source localization of spikes using Champagne, an empirical Bayesian source reconstruction algorithm described previously (Julia P Owen et al., 2012).

2. Method

2.1. The DSSP algorithm

This section introduces the DSSP algorithm briefly; Fig. 1 shows the steps of the DSSP algorithm and details of the derivation can be found in Appendix A. In brief, the DSSP algorithm relies on two subspace definitions. The first definition is based on spatial considerations. Sources of interest are assumed to spatially arise from within the brain. This spatial subspace is therefore defined by the lead-field matrix describing the magnetic field distributions arising from activity from all sources within the brain. The lead-field matrix is taken to construct a projector which allows to split the measured data into two components $\boldsymbol{B}_{in}$ fields given by $\boldsymbol{P}_S\boldsymbol{B}$ which stem from brain sources, and $\boldsymbol{B}_{out}$ fields given by $(\boldsymbol{I}-\boldsymbol{P}_S)\boldsymbol{B}$ which are orthogonal and do not arise from brain sources. The second definition is based on temporal considerations. The temporal representations of $\boldsymbol{B}_{in}$ and $\boldsymbol{B}_{out}$ may not be orthogonal to each other and it is likely that strong interference components that are present in both spatial components $\boldsymbol{B}_{in}$ and $\boldsymbol{B}_{out}$. These interference components can be identified by constructing a temporal subspace projector which is orthogonal to the intersection of the temporal subspaces of $\boldsymbol{B}_{in}$ and $\boldsymbol{B}_{out}$. The final cleaned DSSP data is obtained by projecting the original signal through this temporal subspace operator. The difference between the DSSP and

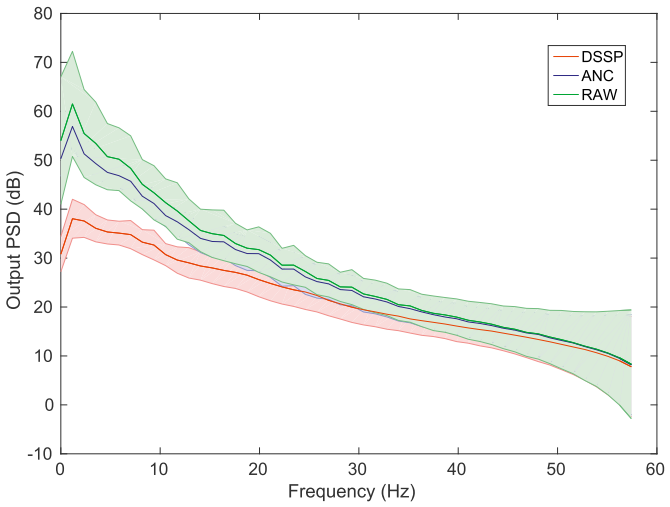

Fig. 3. Averaged power spectral density (PSD) across all channels and subjects, before and after DSSP and ANC.

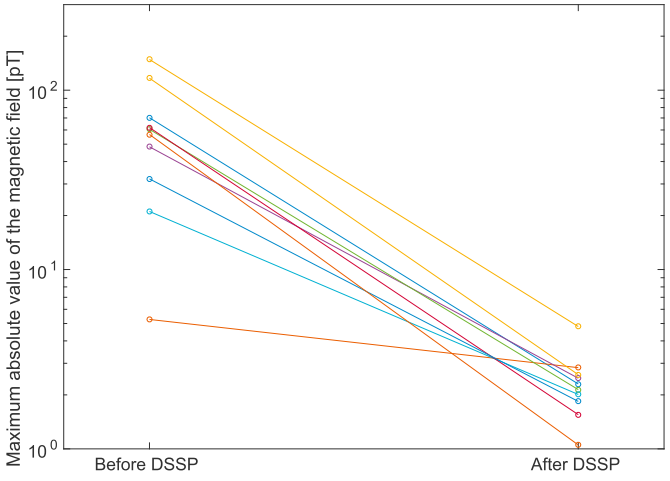

Fig. 4. Maximum absolute value of the magnetic fields across channels and time before and after DSSP for all ten subjects. Note that the y-axis is plotted in log units showing one order of magnitude reduction by DSSP.

the tSSS algorithm is the way of splitting the data into spatial components of $\boldsymbol{B}_{in}$ and $\boldsymbol{B}_{out}$. DSSP uses the lead-field to perform this whereas the tSSS uses spherical harmonic expansions of the magnetic field data.

2.2. Subjects

We selected 10 epilepsy patients with VNS who underwent a clinical MEG study as part of epilepsy surgery evaluation at the University of California, San Francisco (UCSF) Biomagnetic Imaging Laboratory (BIL) between November 24th, 2004 and May 6th, 2016. Prior to MEG, all patients had high-resolution epilepsy protocol 3T T1-MRI scans for coregistration of localized spikes. Table 1 summarizes clinical characteristics of these subjects.

2.3. MEG recordings

Simultaneous EEG and MEG recordings were performed inside a magnetically shielded room with a 275 channel whole-head axial gradiometer system (VSM MedTech, Port Coquitlam, British Columbia). MEG data were recorded from each patient in a passband of 0–75 Hz using a CTF 275 channel whole cortex MEG helmet while simultaneous twenty-one channel scalp EEG data were recorded using a modified international 10–20 system that includes subtemporal electrodes. Thirty to forty minutes of spontaneous data were obtained in intervals of 10–15 min with the patient asleep and awake. The position of the patient's head in the dewar relative to the MEG sensors was determined using indicator coils before and after each recording interval to verify adequate sampling of the entire field. The data were then bandpass filtered offline, initially at 1–70 Hz. More details of the recording methods have been previously described (Nagarajan et al., 2007a). As artifact commonly distorted MEG recordings from the patients with VNS implants, in order to enable for visual analysis and dipole fitting of raw data, additional bandpass filters (typically 10–70 Hz or 20–70 Hz) were applied as needed during analysis of MEG data. After the application of DSSP for artifact removal, all data were bandpass filtered at 1–70 Hz.

2.4. Epileptic spike analysis

Spikes were visually identified by experts - a certified EEG technologist (MM) and a clinical neurophysiologist (JV) - and their results were confirmed by a board-certified clinical neurophysiologist and epileptologist (HEK). To ensure bias-free analysis of data, all reviewers were blinded to the identity of the subject and their clinical data during spike identification and localization procedures. EEG spikes were identified based on the criteria defined by the International Federation of Clinical Neurophysiology (IFCN) (Deuschl Eisenet al., 1999) and the ACMEGS (I Bagic et al., 2011) for EEG epileptiform discharges. MEG spikes were chosen for analysis based on duration ($< 80ms$), morphology, field map, and lack of associated artifact. The onset of each spike was marked as the rising deflection of the first sharp negativity from the baseline and equivalent current dipoles were fit using commercial software provided by CTF Systems (VSM MedTech, Port Coquitlam, British Columbia). Only localized spikes with a goodness of fit higher than 90% were accepted. Co-registration of dipoles to MRI scans was performed using fiducials (nasion and preauricular points) to produce magnetic source images (MSI) of dipoles superimposed on anatomic images. The fitted spike dipoles were then inspected and validated according to their location. Simultaneous EEG during MEG was used to define and confirm spikes on MEG, ascertaining that a signal was not an artifact or another physiologic feature, and also to identify spikes when MEG recordings were heavily contaminated by VNS artifact (ie when MEG data were significantly distorted, spike identification relied heavily on EEG).

2.5. DSSP performance evaluation

In the absence of ground truth data, it is somewhat difficult to evaluate performance in absolute terms. We first examine the average power spectrum of the sensor data before and after DSSP processing. To get a sense of DSSP algorithm performance we compare power spectram obtained following DSSP with those obtained following another interference removal method (Adaptive Noise Canceling, or ANC). Traditionally, ANC makes use of data from reference sensors that collect data containing only the interference but not the signal of interest (Widrow et al., 1975; Adachi et al., 2001). However, in the case of data with VNS implant artifacts reference sensor data is not available. Therefore, as an approximation, for this study we define the reference sensor as the MEG channel with the highest power where artifact dominates, and can be deemed to be an “interference only” reference channel. ANC also uses the idea of subspace projection, where the reference sensor is used to create the temporal span of interference, then data from each sensor is then projected onto the subspace orthogonal to the span of interference. This subspace projection ensures that the contributions from interference to each sensor is eliminated, leaving intact sources of interest. We also compare the interference rejection performance of DSSP and of ANC, by comparing the input and output signal power in each sensor of the array.

After DSSP implementation, cleaned MEG recordings were analyzed as described above (without additional band pass filtering) by three individuals with expertise in interictal spike detection (MM, JV, HEK) who

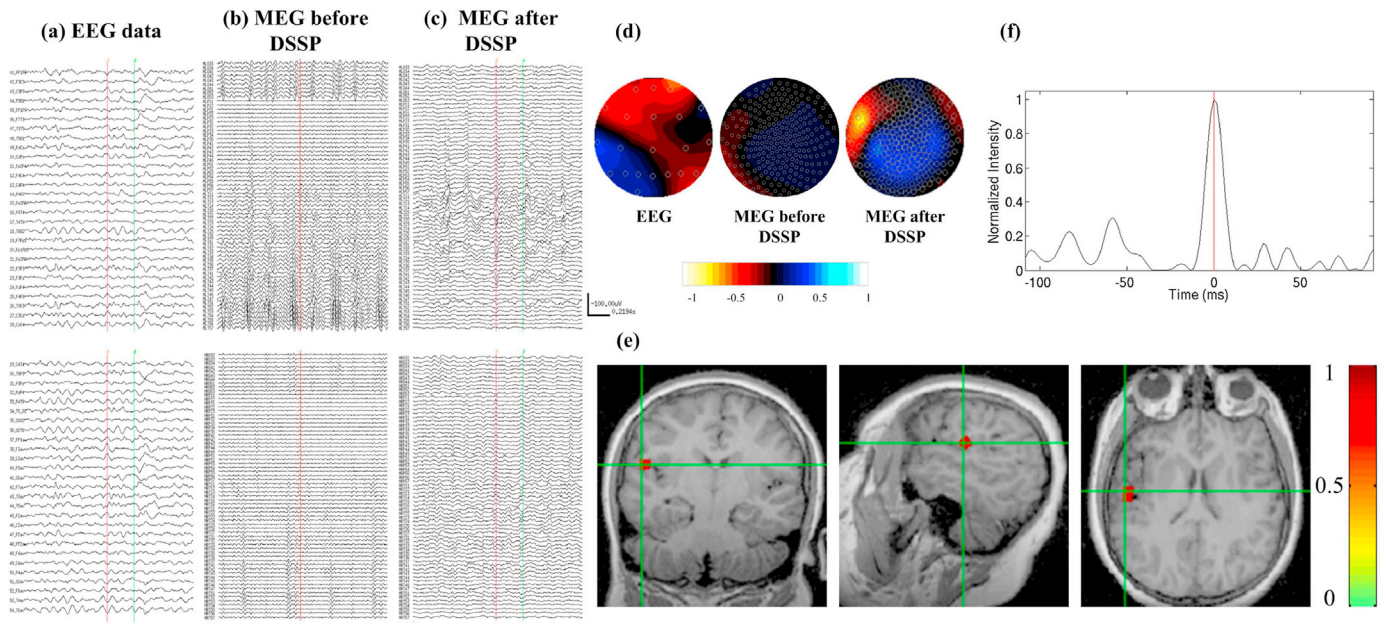

Fig. 5. A representative case showing the effect of the application of DSSP (Subject 5 from Table 1). (a) EEG epoch corresponding to MEG epoch (selected channels) (b) Raw MEG recordings (selected channels) (c) DSSP-processed MEG data. The red line marks a spike not identified in the raw data but seen in the DSSP-processed data, the green line in (a) and (c) mark a different spike. (d) Sensors topographical maps for EEG and MEG at the red line time-point corresponding to the spike (before and after DSSP). (e) Spike localization using Champagne on DSSP-processed data. (f) Normalized intensity for the spike of interest reconstructed through Champagne.

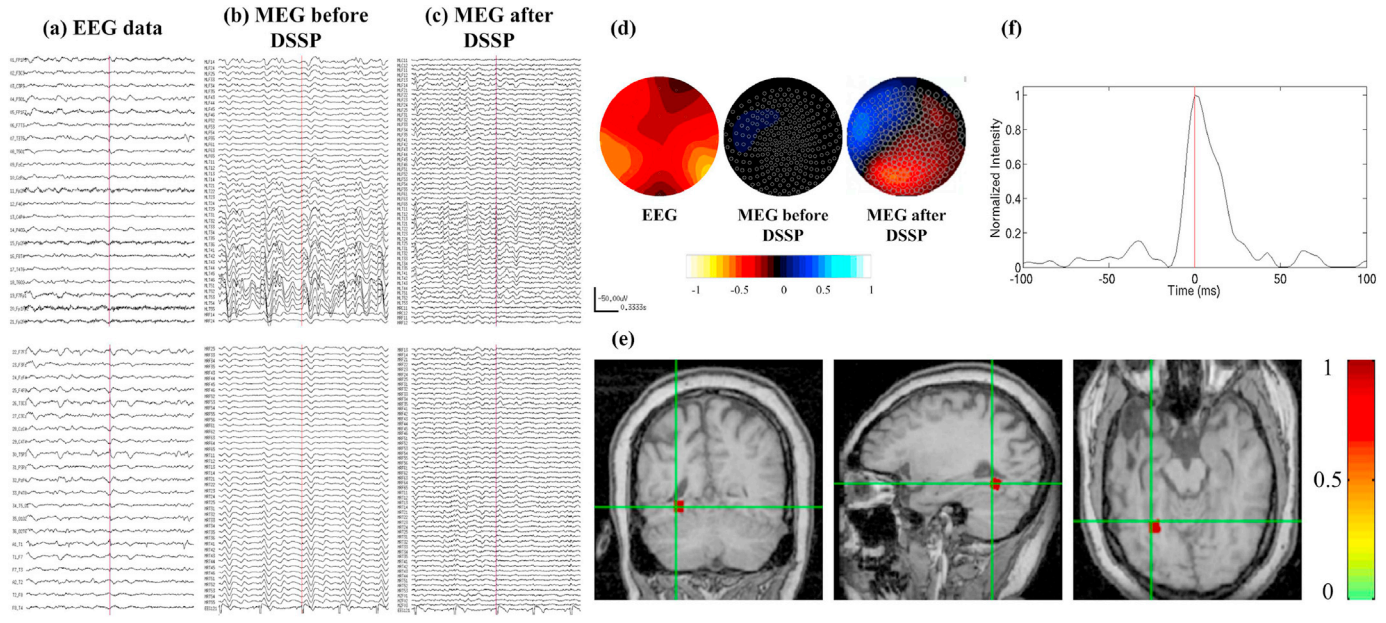

Fig. 6. Another representative case (Subject 4 from Table 1). Legends are identical to the previous figure.

were blinded to the results of the initial (pre-DSSP) analysis. The results were then compared with the original analysis and included quantification of the number of spikes identified and localized, and concordance with other clinical information (EEG, semiology, MRI lesion if present). We also use t-tests to evaluate whether the number of spikes identified and localized were different before and after DSSP.

Finally, DSSP was integrated into a newer source localization pipeline: a united Bayesian framework for MEG/EEG source imaging that includes Variational Bayes Factor Analysis (VBFA) for noise approximation and a Sparse Bayesian Algorithm (Champagne) for source localization (Wipf and Nagarajan, 2009; Wipf et al., 2010), to see whether localization improved upon the incorporation of DSSP algorithm. For each case studied, ten representative spikes seen well on EEG but poorly on MEG in the unprocessed recordings were selected for analysis. For each of the spike selections, Champagne was run for 300 ms (i.e. using 180 data points) on truncated MEG epochs each centered on the selected spike; the required noise estimate input for Champagne was obtained by running VBFA on the 1s of MEG preceding the truncated epoch. The spike source reconstruction map obtained after implementing Champagne was used to judge the performance of DSSP: we observed the activation value of the localized spike activity and the recovered activity time-series, and compared these with standard clinical spike mapping as described above, as well as with correlative clinical data. Across all subjects, we evaluate the consistency of spike localization results with Champagne following

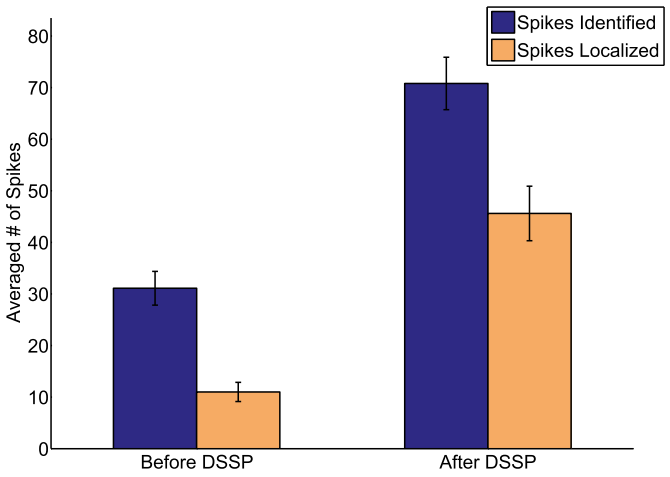

Fig. 7. The averaged number of spikes that could be identified by visual inspection and localized by topographical inspection before and after the application of DSSP for ten subjects with standard error bars.

DSSP processing of data with the presumed epileptogenic zone (based on lesion, ictal EEG, semiology and other clinical data) using a chi-square test.

3. Results

3.1. DSSP vs ANC

We compare the power spectral densities (PSD) before and after artifact rejection with DSSP and ANC algorithms. Fig. 2 shows the PSD for all channels for all ten subjects included in this study. A diagonal line in each panel indicates lack of interference rejection. Although both algorithms show reductions in PSD after processing, in all subjects DSSP shows greater reduction in all channels regardless of the power level in each channel (most red dots are consistently below the diagonal). In contrast, the performance of the ANC algorithm is neither consistent across subjects nor across channels, some channels show negligible reduction in PSD after ANC processing. Upon examination of the PSD as a function of frequency, it is found that the PSD decreases after DSSP and ANC, occur mainly in the low frequency bands from 0 to 30 Hz, with negligible reductions above 30 Hz. However, the reductions in low frequencies are much greater for DSSP when compared to ANC (Fig. 3).

Fig. 4 shows maximum absolute value of the magnetic field strength across channels and time before and after DSSP for each of the ten subjects. Artifact levels were consistently reduced by an order of magnitude, before DSSP the artifact levels were 62.1 pT (62.1 ± 13.55) and were reduced to 2.4 pT (2.4 ± 0.32) after DSSP processing (Fig. 4). This reduction of 96.13% was highly statistically significant (two-tailed paired *t*-test, t-value = 4.40777, p-value = .00034).

3.2. Expert detection and localization of interictal spikes

After the application of the DSSP algorithm to MEG data from people with intractable epilepsy and VNS, both spikes that were well seen on EEG, and those seen primarily on MEG could be visually identified by experts from MEG background at a high rate. Fig. 5 shows EEG data (a) and MEG data (b) from a patient with intractable epilepsy and a VNS implant. It features VNS artifact with partial periodicity, low frequency and high amplitude. After DSSP is applied, as shown in (c), this periodic feature is greatly diminished and the background looks similar to that of most people with epilepsy who do not have VNS. Fig. 5(d) shows sensors topographical maps for MEG after DSSP and EEG maps. Fig. 6 shows similar data for another patient. Fig. 7 shows the average number of spikes that could be identified by visual inspection of the MEG and the average number of spikes that could be localized by topographical inspection before and after DSSP. Over twice as many spikes could be identified after DSSP when compared to before DSSP ($p = 0.037$), and over four times as many spikes could be localized after DSSP when compared to before DSSP ($p = 0.007$).

Source localization of identified interictal spikes in MEG data before DSSP with the Champagne algorithm resulted in localization failure in nine out of the ten cases; in all these cases either no strong activation could be found, or the activity was localized to unusual positions (e.g. near or outside of the skull), and the activity time-series recovered did not resemble that of a spike. However, localization results with Cham-

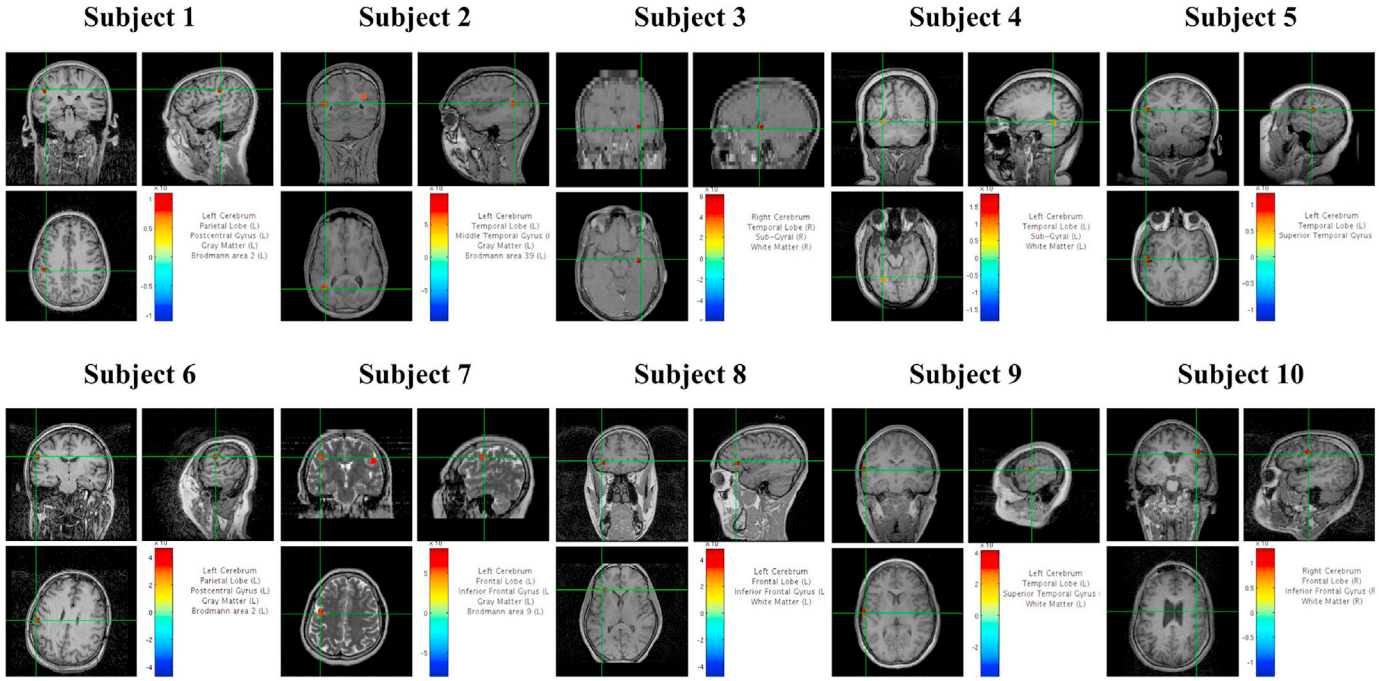

Fig. 8. Source localization results for all ten subjects using Champagne after DSSP.

pagne on MEG data after DSSP resulted in marked improvement. Figs. 5(e) and 6(e) show source localization, and Figs. 5(f) and 6(f) show respective Champagne time series for the spike of interest in the two cases previously discussed. In Fig. 8, all cases could be localized correctly after running DSSP. A Chi-Square test comparing the number of localizations before and after DSSP that are consistent or inconsistent with the presumed epileptogenic zone demonstrates that Champagne localizations were clearer and more consistent after DSSP ($\chi^2 = 16.364$ and $p = 0.0001$).

In order to quantify the accuracy of spatial localization of spikes with the Champagne algorithm after DSSP, we evaluated the cluster radius for ten representative spikes from each subject (to prevent biases for subjects with a greater number of spikes). The averaged radius of the spatial clusters of interictal spikes after DSSP is 13.3 mm (SEM = 1.3) (note that the resolution of the forward model is 8 mm), thus indicating the high accuracy and precision of spike localization with Champagne after DSSP.

4. Discussion

In this study, DSSP was evaluated using typical clinical data from people with epilepsy and VNS, showing its potential to diminish the influence of interference. DSSP processing of MEG data enabled better visual identification of spikes, making meaningful the MEG recordings that were contaminated and previously of limited value. Finally, when integrated with the Champagne source reconstruction algorithm, DSSP did help to achieve more reasonable spike localizations and meaningful recovered spike activity time series. The successful rejection of VNS artifact using DSSP should therefore improve treatment (including surgical planning for resection or other localized therapies) of people with intractable epilepsy and VNS. Given these results, as we gain further experience with DSSP, its potential use in the setting of other interference types can also be explored.

Analysis of the power spectrum of sensor data revealed that DSSP resulted in greater reductions in lower frequency bands when compared to an adaptive noise cancelation benchmark. However, in future a more detailed comparison of performance with other benchmark algorithms including the tSSS algorithm is warranted (Taulu and Hari, 2009).

There are several limitations to this study. First, small sample size could potentially limit the generalizability of our results. However, we included all patients who had VNS implants in our study. Second, this is a retrospective and non-randomized study. Currently, for new cases with VNS artifact, we are undertaking a prospective study applying DSSP prior to initial analysis, and results of this prospective study will be published in the future. Finally, although better localization was achieved with the addition of DSSP to Champagne, whether this truly improved outcomes as a results of epileptogenic zone mapping is unknown. Additional information about the true epileptogenic zone (e.g. from follow-up after resective surgery) will be needed to make such judgments. Therefore, we can only conclude that DSSP helps achieve spike mapping, but cannot evaluate the impact of localization accuracy on outcome. We are collecting follow-up information from patients who went through surgery after MEG recording, and in future this information could be used as a gold standard to judge the performance of DSSP.

Indeed, DSSP will not perform good artifact rejection if the sources are located close to the brain and if the artifacts are correlated with brain activity. The DSSP algorithm is suited to remove interferences from sources located fairly close to the boundary of the source space. The eyeblink and cardiac artifacts encountered in MEG measurements are also such interferences.

5. Conclusion

In short, DSSP is a novel interference rejection algorithm worth exploration. The retrospective clinical study has shown its potential to deal with high amplitude, periodic interference currently not handled well by other algorithms. DSSP helped to recover distorted MEG recordings from people with intractable epilepsy and VNS implants, making epileptic spike identification easier and spike mapping better. The specificity of this improved spike mapping is still unknown.

Acknowledgment

The authors would like to thank Susanne Honma, Danielle Mizuiri and Anne Findlay for collecting much of the MEG data in the Biomagnetic Imaging Laboratory. We would also like to thank Mary Mantle for blinded analysis of some of the MEG data. This work was supported by NIH grants R01EB022717, R01DC013979, UCOP MRP-17-454755, and a gift from Ricoh Company Ltd..

Appendix A. Derivation of DSSP

Appendix A.1. Data model

This section briefly describes the DSSP algorithm. A full explanation of the algorithm is available in (Sekihara et al., 2016). Also, a detailed explanation of the DSSP algorithm in the context of the time-domain signal subspace can be found in (Sekihara and Nagarajan, 2017). Let us define the measurement of the m-th sensor at time t as $y_m(t)$. The measurement from the whole sensor array is expressed as a column vector $\boldsymbol{y}(t)$: $\boldsymbol{y}(t) = [y_1(t), y_2(t), \ldots, y_M(t)]^T$, which is called the data vector. Here, M is the number of sensors, and the superscript T indicates the matrix transpose. Let us assume that a unit-magnitude source exists at $\boldsymbol{r}$ ($\boldsymbol{r} = (x,y,z)$). When this unit-magnitude source is directed in the x, y, and z directions, the outputs of the m-th sensor are respectively denoted as $l_m^x(\boldsymbol{r})$, $l_m^y(\boldsymbol{r})$, and $l_m^z(\boldsymbol{r})$. Let us define an $M \times 3$ matrix $\boldsymbol{L}(\boldsymbol{r})$ whose m-th row is equal to a 1×3 row vector $[l_m^x(\boldsymbol{r}), l_m^y(\boldsymbol{r}), l_m^z(\boldsymbol{r})]$. This matrix $\boldsymbol{L}(\boldsymbol{r})$, referred to as the lead field matrix, represents the sensitivity of the sensor array at $\boldsymbol{r}$.

The DSSP algorithm was proposed in order to remove interfering magnetic fields overlapped onto signal magnetic fields. The algorithm assumes the data model:

$$\boldsymbol{y}(t) = \boldsymbol{y}_S(t) + \boldsymbol{y}_I(t) + \boldsymbol{\varepsilon}, \tag{A.1}$$

where $\boldsymbol{y}_S(t)$, (called the signal vector), represents the signal of interest, $\boldsymbol{y}_I(t)$, (called the interference vector), represents the interference magnetic field, and $\boldsymbol{\varepsilon}$, (called the random vector), represents additive sensor noise. We denote the time series outputs of a sensor array $\boldsymbol{y}(t_1), \ldots, \boldsymbol{y}(t_K)$, where K is the total number of measured time points. The measured data matrix $\boldsymbol{B}$ is thus defined as: $\boldsymbol{B} = [\boldsymbol{y}(t_1), \ldots, \boldsymbol{y}(t_K)]$ The signal matrix is defined as $\boldsymbol{B}_S = [\boldsymbol{y}_S(t_1), \ldots, \boldsymbol{y}_S(t_K)]$, and the interference matrix as $\boldsymbol{B}_I = [\boldsymbol{y}_I(t_1), \ldots, \boldsymbol{y}_I(t_K)]$ Then, the data model in Eq. (A.1) is expressed in a matrix form as:

$$\boldsymbol{B} = \boldsymbol{B}_S + \boldsymbol{B}_I + \boldsymbol{B}_\varepsilon, \tag{A.2}$$

where $\boldsymbol{B}_e$ is the noise matrix whose j-th column is equal to the noise vector $\boldsymbol{\varepsilon}$ at time t_j.

Appendix A.2. Pseudo-signal subspace projector

The dual signal space projection (DSSP) algorithm assumes that the interference sources are located outside the source space which indicates a region in which signal sources can exist. The DSSP algorithm uses the so-called pseudo-signal subspace projector, and to derive it, voxels are defined over the source space, in which the voxel locations are denoted $\boldsymbol{r}_1, \ldots, \boldsymbol{r}_N$. The augmented leadfield matrix over these voxel locations is defined as

$$\boldsymbol{F} = [\boldsymbol{L}(\boldsymbol{r}_1), \ldots, \boldsymbol{L}(\boldsymbol{r}_N)], \tag{A.3}$$

and the pseudo-signal subspace $\breve{\mathscr{E}}_S$ is defined such that

$$\breve{\mathscr{E}}_S = \mathrm{csp}(\boldsymbol{F}), \tag{A.4}$$

where the notation $\mathrm{csp}(\boldsymbol{X})$ indicates the column space of a matrix $\boldsymbol{X}$. If the voxel interval is sufficiently small and voxel discretization errors are negligible, we have the relationship $\breve{\mathscr{E}}_S \supset \mathscr{E}_S$ where $\mathscr{E}_S$ indicates the true signal subspace. Therefore, a vector contained in the signal subspace is also contained in the pseudo-signal subspace.

Let us derive the orthonormal basis vectors of the pseudo-signal subspace. To do so, we compute the singular value decomposition of $\boldsymbol{F}$:

$$\boldsymbol{F} = \sum_{j=1}^{M} \lambda_j \boldsymbol{e}_j \boldsymbol{f}_j^T, \tag{A.5}$$

where $\boldsymbol{e}_j$ and $\boldsymbol{f}_j$ are left and right singular vectors. In Eq. (A.5), we assume the relationship $M < N$, and the singular values are numbered in a decreasing order. If the singular values $\lambda_1, \ldots, \lambda_\tau$ are distinctively large and other singular values $\lambda_{\tau+1}, \ldots, \lambda_M$ are nearly equal to zero, the leading τ singular vectors $\boldsymbol{e}_1, \ldots, \boldsymbol{e}_\tau$ form orthonormal basis vectors of the pseudo-signal subspace $\breve{\mathscr{E}}_S$. Thus, the projector onto $\breve{\mathscr{E}}_S$ is obtained using

$$\boldsymbol{P}_S = [\boldsymbol{e}_1, \ldots, \boldsymbol{e}_\tau][\boldsymbol{e}_1, \ldots, \boldsymbol{e}_\tau]^T. \tag{A.6}$$

Note that $(\boldsymbol{I} - \boldsymbol{P}_S)\boldsymbol{y}_S(t) = (\boldsymbol{I} - \boldsymbol{P}_S)\boldsymbol{B}_S = 0$ holds.

Appendix A.3. DSSP algorithm

The DSSP algorithm applies $\boldsymbol{P}_S$ and $\boldsymbol{I} - \boldsymbol{P}_S$ to the data matrix $\boldsymbol{B}$ to create two kinds of data matrices:

$$\boldsymbol{P}_S\boldsymbol{B} = \boldsymbol{B}_S + \boldsymbol{P}_S\boldsymbol{B}_I + \boldsymbol{P}_S\boldsymbol{B}_\varepsilon, \tag{A.7}$$

$$(\boldsymbol{I} - \boldsymbol{P}_S)\boldsymbol{B} = (\boldsymbol{I} - \boldsymbol{P}_S)\boldsymbol{B}_I + (\boldsymbol{I} - \boldsymbol{P}_S)\boldsymbol{B}_\varepsilon. \tag{A.8}$$

Let us use the notation $\mathrm{rsp}(\boldsymbol{X})$ to indicate the row space of a matrix $\boldsymbol{X}$. Then, the relationships, $\mathrm{rsp}(\boldsymbol{P}_S\boldsymbol{B}_I) = \mathscr{K}_I$, $\mathrm{rsp}((\boldsymbol{I} - \boldsymbol{P}_S)\boldsymbol{B}_I) = \mathscr{K}_I$, and $\mathrm{rsp}(\boldsymbol{B}_S) = \mathscr{K}_S$ hold, where $\mathscr{K}_S$ and $\mathscr{K}_I$ respectively indicate the time-domain signal and interference subspaces. According to arguments in (Sekihara and Nagarajan, 2017), we can finally derive the relationship:

$$\mathscr{K}_I \supset \mathrm{rsp}(\boldsymbol{P}_S\boldsymbol{B}) \cap \mathrm{rsp}((\boldsymbol{I} - \boldsymbol{P}_S)\boldsymbol{B}). \tag{A.9}$$

The equation above shows that the intersection between $\mathrm{rsp}(\boldsymbol{P}_S\boldsymbol{B})$ and $\mathrm{rsp}((\boldsymbol{I} - \boldsymbol{P}_S)\boldsymbol{B})$ forms a subset of the interference subspace $\mathscr{K}_I$. The basis vectors of the intersection can be derived using the algorithm described in (Gene et al., 2012). Once the orthonormal basis vectors of the intersection $\boldsymbol{\psi}_1, \ldots, \boldsymbol{\psi}_r$ are obtained, we can compute the projector onto the intersection $\boldsymbol{\Pi}_I$ such that

$$\boldsymbol{\Pi}_I = [\boldsymbol{\psi}_1, \ldots, \boldsymbol{\psi}_r][\boldsymbol{\psi}_1, \ldots, \boldsymbol{\psi}_r]^T. \tag{A.10}$$

Using this $\boldsymbol{\Pi}_I$ as the projector onto the (time-domain) interference subspace $\mathscr{K}_I$, the interference removal is achieved and the signal matrix is estimated by the time-domain signal space projection (Sekihara and Nagarajan, 2017), which is

$$\widehat{\boldsymbol{B}}_S = \boldsymbol{B}(\boldsymbol{I} - \boldsymbol{\Pi}_I) = \boldsymbol{B}\big(\boldsymbol{I} - [\boldsymbol{\psi}_1, \ldots, \boldsymbol{\psi}_r][\boldsymbol{\psi}_1, \ldots, \boldsymbol{\psi}_r]^T\big). \tag{A.11}$$

The method of removing the interference in a manner described above is called dual signal space projection (DSSP). Note that since the basis vectors of the intersection, $\boldsymbol{\psi}_1, \ldots, \boldsymbol{\psi}_r$, span only a subset of the interference subspace $\mathscr{K}_I$, this method cannot perfectly remove interferences. However, when the intersection $\mathrm{rsp}(\boldsymbol{P}_S\boldsymbol{B}) \cap \mathrm{rsp}((\boldsymbol{I} - \boldsymbol{P}_S)\boldsymbol{B})$ is a reasonable approximation of $\mathscr{K}_I$, interferences can effectively be removed by the DSSP algorithm.

References

Adachi, Y., Shimogawara, M., Higuchi, M., Haruta, Y., Ochiai, M., 2001. Reduction of non-periodic environmental magnetic noise in MEG measurement by continuously adjusted least squares method. IEEE Trans. Appl. Supercond. 11 (1), 669–672.

de Cheveigné, Alain, Parra, Lucas C., 2014. Joint decorrelation, a versatile tool for multichannel data analysis. Neuroimage 98, 487–505.

Deuschl, Günther, Eisen, Andrew, et al., 1999. Recommendations for the Practice of Clinical Neurophysiology: Guidelines of the International Federation of Clinical Neurophysiology.

Gene, H., Golub, Van Loan, Charles F., 2012. In: Matrix Computations, Volume 3. The Johns Hopkins University Press.

I Bagic, Anto, Knowlton, Robert C., Rose, Douglas F., Ebersole, John S., ACMEGS Clinical Practice Guideline (CPG) Committee, et al., 2011. American clinical

magnetoencephalography society clinical practice guideline 1: recording and analysis of spontaneous cerebral activity. J. Clin. Neurophysiol. 28 (4), 348–354.
Owen, Julia P., Wipf, David P., Attias, Hagai T., Sekihara, Kensuke, Nagarajan, Srikantan S., 2012. Performance evaluation of the champagne source reconstruction algorithm on simulated and real M/EEG data. Neuroimage 60 (1), 305–323.
Nagarajan, Srikantan S., Attias, Hagai T., Hild II, Kenneth E., Sekihara, Kensuke, 2006. A graphical model for estimating stimulus-evoked brain responses from magnetoencephalography data with large background brain activity. Neuroimage 30 (2), 400–416.
Nagarajan, Srikantan S., Attias, Hagai T., Sekihara, Kensuke, Hild, Kenneth E., 2006. Partitioned factor analysis for interference suppression and source extraction. In: International Conference on Independent Component Analysis and Signal Separation. Springer, pp. 189–197.
Nagarajan, Srikantan S., Attias, Hagai T., Hild, Kenneth E., Sekihara, Kensuke, 2007. A probabilistic algorithm for robust interference suppression in bioelectromagnetic sensor data. Stat. Med. 26 (21), 3886–3910.
Nagarajan, S.S., Attias, H.T., Hild, K. Ee, Sekihara, K., 2007. A probabilistic algorithm for robust interference suppression in bioelectromagnetic sensor data. Stat. Med. 26, 3886–3910.
Ossadtchi, A., Baillet, S., Mosher, J.C., Thyerlei, D., Sutherling, W., Leahy, R.M., 2004. Automated interictal spike detection and source localization in magnetoencephalography using independent components analysis and spatio-temporal clustering. Clin. Neurophysiol. 115 (3), 508–522.
Sekihara, K., Nagarajan, S.S., 2017. Subspace-based interference removal methods for a multichannel biomagnetic sensor array. J. Neural. Eng. 14 (5), 051001.
Sekihara, Kensuke, Kawabata, Yuya, Ushio, Shuta, Sumiya, Satoshi, Kawabata, Shigenori, Adachi, Yoshiaki, Nagarajan, Srikantan S., 2016. Dual signal subspace projection (DSSP): a novel algorithm for removing large interference in biomagnetic measurements. J. Neural. Eng. 13 (3), 036007.
Taulu, Samu, Hari, Riitta, 2009. Removal of magnetoencephalographic artifacts with temporal signal-space separation: demonstration with single-trial auditory-evoked responses. Hum. Brain Mapp. 30 (5), 1524–1534.
Taulu, Samu, Simola, Juha, 2006. Spatiotemporal signal space separation method for rejecting nearby interference in MEG measurements. Phys. Med. Biol. 51 (7), 1759.
Widrow, Bernard, Glover, John R., McCool, John M., Kaunitz, John, Williams, Charles S., Hearn, Robert H., Zeidler, James R., Dong, JR Eugene, Goodlin, Robert C., 1975. Adaptive noise cancelling: principles and applications. Proc. IEEE 63 (12), 1692–1716.
Wipf, David, Nagarajan, Srikantan, 2009. A unified bayesian framework for MEG/EEG source imaging. Neuroimage 44 (3), 947–966.
Wipf, David P., Owen, Julia P., Attias, Hagai T., Sekihara, Kensuke, Nagarajan, Srikantan S., 2010. Robust bayesian estimation of the location, orientation, and time course of multiple correlated neural sources using MEG. Neuroimage 49 (1), 641–655.
Zumer, Johanna M., Attias, Hagai T., Sekihara, Kensuke, Nagarajan, Srikantan S., 2008. Probabilistic algorithms for MEG/EEG source reconstruction using temporal basis functions learned from data. Neuroimage 41 (3), 924–940.